Quantum effects in warp drives

Stefano Finazzi[1,a]

[1]*INO-CNR BEC Center and Dipartimento di Fisica, Universita di Trento, via Sommarive 14, 38123 Povo-Trento, Italy*

Abstract. Warp drives are interesting configurations that, at least theoretically, provide a way to travel at superluminal speed. Unfortunately, several issues seem to forbid their realization. First, a huge amount of exotic matter is required to build them. Second, the presence of quantum fields propagating in superluminal warp-drive geometries makes them semiclassically unstable. Indeed, a Hawking-like high-temperature flux of particles is generated inside the warp-drive bubble, which causes an exponential growth of the energy density measured at the front wall of the bubble by freely falling observers. Moreover, superluminal warp drives remain unstable even if the Lorentz symmetry is broken by the introduction of regulating higher order terms in the Lagrangian of the quantum field. If the dispersion relation of the quantum field is subluminal, a black-hole laser phenomenon yields an exponential amplification of the emitted flux. If it is superluminal, infrared effects cause a linear growth of this flux.

1 Introduction

A warp drive [1] can be defined as a bubble of spacetime moving in an asymptotically flat spacetime at an arbitrary speed. This configuration provides both a way to travel at superluminal speeds and an exciting ground to test our comprehension of general relativity (GR) and quantum field theory in curved spacetimes (for instance when investigating warp-drive implications for causality [2]). Their geometry is defined by the line element

$$ds^2 = -c^2 dt^2 + [dx - v(r)dt]^2 + dy^2 + dz^2, \tag{1}$$

where $r \equiv \sqrt{(x - v_0 t)^2 + y^2 + z^2}$ parametrizes the distance from the center of the bubble and v_0 is the warp-drive velocity. The function v satisfies $v(0) = v_0$ and $v(r) \to 0$ for $r \to \infty$.

When this metric is put into Einstein's equations, it is apparent that a large amount of exotic matter (i.e., matter that violates energy conditions, see Ref. [3] for a complete review about "exotic spacetimes") is required to stretch the spacetime around the warp-drive bubble. Surprisingly, exotic matter is needed to sustain warp drives moving not only with superluminal speeds, but also with subluminal ones [4, 5]. Furthermore, the amount of exotic matter is related to both the size of the warp-drive bubble and the thickness of the bubble walls [6]. If the exoticity is provided by quantum fields, satisfying therefore the so-called quantum inequalities (QI—see [7] for a review about QI applied to exotic spacetimes), then the violations of the energy conditions must be confined to Planck-size

---

[a]e-mail: finazzi@science.unitn.it

regions. Accordingly, the thickness Δ of the wall of the bubble is of Planck size [$\Delta \leq 10^2 (v_0/c) L_P$, where L_P is the Planck length]. Unfortunately, to support a warp-drive bubble with such thin walls, a size of about 100 m, and propagating at $v_0 \approx c$, a huge amount of exotic matter is required, $|E_-| \gg 10^{11} M_\odot$. Modified configurations with a reduced surface area but the same bubble volume [8] can reduce the amount of negative energy ($|E_-| \approx 0.3 M_\odot$ for a 100 m-radius bubble), although some positive energy must be added outside the bubble ($E_+ \approx 2.5 M_\odot$).

Regarding the feasibility of warp-drive configurations, a parallel line of research has focused on the study of their semiclassical stability against the introduction of quantum fields propagating on these geometries. In Ref. [9] this issue was studied in the case of an eternal superluminal warp drive. It was noticed that, for an observer within the warp-drive bubble, the backward and forward walls (along the direction of motion) look like the horizon of a black hole and of a white hole, respectively. By imposing a quantum state which is vacuum at the null infinities (that is, the analog of the Boulware state for an eternal black hole) it was found that the renormalized stress-energy tensor (RSET) diverges at the horizons (see Ref. [10] for a different point of view). Thus, the divergence of the RSET at the horizons makes superluminal warp drives unstable within the context of semiclassical GR.

In a more realistic situation, a warp drive is dynamically created at a finite time t_H with a very low velocity and then accelerated to superluminal speeds. In this case the quantum state is globally fixed by suitable boundary conditions at early times, before the formation of the warp-drive bubble. This situation is similar to the formation of a black hole through a gravitational collapse. In the black hole case, the globally defined quantum state that is vacuum on $\mathscr{I}^-$ is regular on the horizon and thermal on $\mathscr{I}^+$. In other words, the dynamics of a collapse end up selecting a quantum state that at late times resembles the Unruh state defined on eternal black holes, rather than a Boulware-like state.

In this contribution we summarize the results of three works [11–13] investigating the semiclassical stability properties of warp drives. In Sec. 2 we analyze the causal structure on an eternal warp drive and of a warp drive which is dynamically created with zero velocity and then accelerated up to superluminal speed in a finite amount of time. In this latter configuration, where a proper quantum state can be unambiguously defined, we investigate the properties of spontaneous quantum vacuum emission by calculating the RSET inside the warp-drive bubble (Sec. 3). In the center of the bubble we find a thermal flux at the Hawking temperature corresponding to the surface gravity of the black horizon. Furthermore, the RSET grows exponentially with time on the white horizon. This makes warp drives unstable once superluminal speeds are reached.

However, this analysis rests on relativistic quantum field theory. Thus, one may wonder whether this instability is peculiar to the assumed local Lorentz symmetry. For instance, it is known that non-linear dispersion relations remove Cauchy horizons and regulate the fluxes emitted by white holes [14]. To clarify this issue, in Sec. 4, this stability analysis is extended to a quantum field theory where Lorentz invariance is broken at ultra-high energy [13]. Even if the exponential growth of the RSET on the white hole is in fact removed, new types of instability appear, whose properties depend on the form of the dispersion relation of the quantum field.

2 The warp-drive geometry

2.1 Causal structure

The geometrical and causal properties of warp-drive spacetimes are more conveniently investigated by restricting to the 1 + 1 dimensional case using a new spatial coordinate $r \equiv x - v_0 t$ in the metric of Eq. (1),

$$ds^2 = -c^2 dt^2 + [dr - \bar{v}(r)dt]^2 , \tag{2}$$

where $\bar{v} = v - v_0$. We put $v = v_0 f(r)$, where $f(r)$ is a smooth function with maximum $f(0) = 1$ and $f(r) \to 0$ for $r \to \pm\infty$. Therefore, $\bar{v}$ has a maximum in $r = 0$, where it vanishes, and goes to the constant value $-v_0 < -c$ for $r \to \pm\infty$. Consequently there are two positions r_B and r_W where $|\bar{v}| = c$. A possible choice of $\bar{v}$ satisfying these conditions is plotted in Fig. 1. As seen from an observer inside the bubble, r_B and r_W correspond to a black and a white hole horizons, $\mathcal{H}_B$ and $\mathcal{H}_W$, respectively, separating the spacetime in three regions: L, appearing as the interior of the black hole, C, appearing as the exterior of both the black and the white hole, and R, appearing as the interior of the white hole (see Fig. 1).
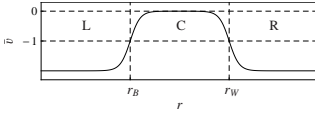

Figure 1. Velocity profile for a rightgoing warp drive [see Eq.(2)]. Two *superluminal* asymptotic regions L and R are separated by a black and a white horizon from a compact internal *subluminal* region C. The Killing field ∂_t is space-like in L and R, light-like on both horizons, and time-like in C.
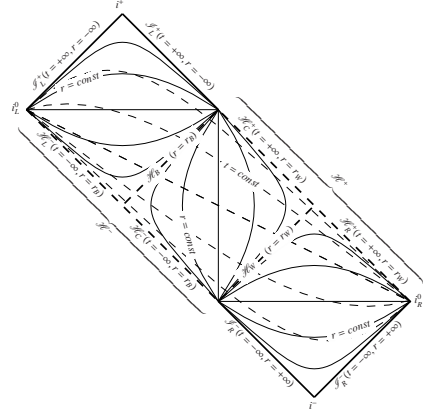

Figure 2. Penrose diagram of an eternal warp drive. Lines of constant r (solid lines) and of constant t (dashed lines). Future and past horizons at $r = r_{B,W}$ (heavy dashed lines). The geometry can be extended to the future of $\mathcal{H}^+$ (formed by $\mathcal{H}_C^+$ and $\mathcal{H}_R^+$) and to the past of $\mathcal{H}^-$ (formed by $\mathcal{H}_C^-$ and $\mathcal{H}_L^-$).

The Penrose diagram of a warp drive is therefore obtained by pasting together the diagrams of a black hole, on the left, and of a white hole, on the right. Note that this diagram does not represent the maximal analytical extension of this spacetime: The dashed lines $\mathcal{H}^-$ (formed by $\mathcal{H}_C^-$ and $\mathcal{H}_L^-$) and $\mathcal{H}^+$ (formed by $\mathcal{H}_C^+$ and $\mathcal{H}_R^+$) signal the locations at which the geometry can be extended. $\mathcal{H}_C^-$ and $\mathcal{H}_C^+$ correspond to the past and future horizons in the Penrose diagrams of an eternal black and white hole, respectively. While in the black hole case a maximal extension is well known for vacuum solutions such as the Schwarzschild or Kerr spacetimes, for a warp-drive geometry the maximal extension cannot be uniquely determined because the distribution of matter is unknown beyond $\mathcal{H}^\pm$, which behave like Cauchy horizons.

Hence, because of the presence of the past Cauchy horizon $\mathcal{H}^-$, a quantum state with appropriate initial conditions cannot be imposed at $t \to -\infty$. However, in a realistic situation, a warp-drive geometry is not eternal but it is dynamically formed at some finite time t_H. Before t_H the causal structure of the spacetime is Minkowskian and proper boundary conditions can be chosen.

This dynamical warp-drive geometry is described by a metric of the form of Eq. (2), by replacing the constant velocity $\bar{v}$ with a time dependent velocity $\hat{v}(t, r)$, satisfying $\hat{v}(t, r) \to 0$, for $t \to -\infty$ and $\hat{v}(t, r) \to \bar{v}(r)$, for $t \to +\infty$. The corresponding Penrose diagram, obtained by interpolating between these two behaviors, is plotted in Fig. 3. The causal structure is initially Minkowskian ($\hat{v} = 0$). Then

it progressively changes till $t = t_H$, when the horizon forms. After t_H, the Penrose diagram coincides with that of a stationary warp drive (Fig. 2). With respect to the eternal case, the past Cauchy horizon $\mathcal{H}^-$ has disappeared but the geometry can still be extended in the future, beyond the Cauchy horizons $\mathcal{H}_C^+$ and $\mathcal{H}_R^+$. There exist indeed observers moving on time-like lines that reach $\mathcal{H}_C^+$ and $\mathcal{H}_R^+$ in a finite proper time.
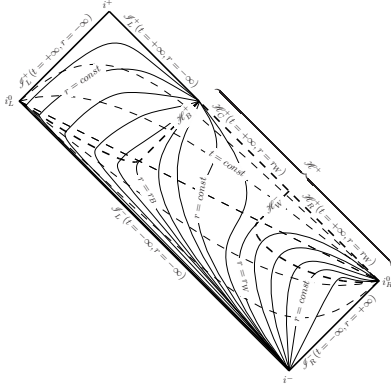

Figure 3. Penrose diagram of a dynamic warp drive. Lines of constant r (solid lines) and of constant t (dashed lines). The lines of constant r become null at the apparent horizons (heavy dashed lines).
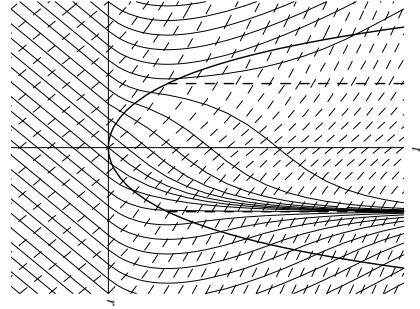

Figure 4. Light rays propagating rightward (solid lines) and leftward (dashed lines) in the plane (t, r) in a warp-drive spacetime defined by the velocity profile of Eq. (3). Heavy solid lines represent the functions $r(t) = \pm \xi(t) = \pm \mathrm{arccosh}(t+1)$ used to implement the dynamical formation of the warp drive. At $t < 0$ the metric is Minkowskian. The horizons at r_B and r_W (heavy dashed lines) appear at $t_H = 1$.

2.2 Light-ray propagation

The presence of a black hole horizon in a superluminal warp-drive geometry suggests the possibility that Hawking-like radiation is produced. To investigate this phenomenon, we first study how light rays are bent by the warp-drive geometry, in particular we determine the relation $U = p(u)$ between past U and future u null affine coordinates [15]. This information is indeed sufficient to investigate the properties of particle creation [16]. For illustrative purposes, in Fig. 4 we plot the rightgoing (solid line) and leftgoing (dashed lines) null geodesics propagating in a warp-drive geometry, defined by the following velocity profile ($c = 1$),

$$\hat{v}(r, t) = \begin{cases} 0 & \text{if } t \leq 0, \\ \bar{v}[\xi(t)] & \text{if } t > 0 \text{ and } |r| \geq \xi(t), \\ \bar{v}(r) & \text{if } t > 0 \text{ and } |r| < \xi(t), \end{cases} \tag{3}$$

with

$$\xi(t) = \mathrm{arccosh}(t + 1) \tag{4}$$

and

$$\bar{v}(r) = 2\left[\frac{1}{\cosh(r)} - 1 \right]. \tag{5}$$

As required, $\hat{v}(r, t)$ smoothly interpolates between a Minkowski metric ($\hat{v} = 0$) at early times ($t < 0$) and a warp-drive geometry defined by $\bar{v}$. The horizons appear at $t_H = 1$.

To determine the general relation $U = p(u)$, we start from the differential equation for the propagation of rightgoing light rays

$$\frac{\mathrm{d}r}{\mathrm{d}t} = c + \hat{v}(r, t). \tag{6}$$

Since for $t \gg t_H$ the velocity profile $\hat{v} = \bar{v}$ depends only on r, the late-time null coordinate u is defined by

$$\mathrm{d}u = \mathrm{d}t - \frac{\mathrm{d}r}{c + \bar{v}(r)}. \tag{7}$$

We now restrict to the central region C. Here the asymptotic form is found by integrating the above equation in the limit $r \to r_{B,W}$, where the velocity $\bar{v}$ is

$$\bar{v} = -c \pm \kappa_{B,W} (r - r_{B,W}) + O\left((r - r_{B,W})^2\right) \tag{8}$$

and

$$\kappa_{B,W} \equiv \left.\frac{\mathrm{d}\bar{v}}{\mathrm{d}r}\right|_{r=r_{B,W}} \tag{9}$$

are the surface gravities of the black horizon and of the white horizon, respectively. For the sake of simplicity, from now on we assume that they have the same value $\kappa_{B,W} = \kappa$, without loss of generality. We obtain

$$u \simeq t \mp \frac{1}{\kappa} \ln \left| r - r_{B,W} \right|. \tag{10}$$

The early-time null coordinate U, obtained by integrating Eq. (6) when $\hat{v} = 0$, reduces to

$$U(t \to -\infty) = t - \frac{r}{c}, \tag{11}$$

in the limit $t \to \infty$. This coordinate is regular everywhere, in particular on the horizons. Consequently, on a t slice in the late-time stationary region, U can be written as

$$U_{B,W} = \mathcal{U}_{B,W} (r - r_{B,W}), \tag{12}$$

where $U_{B,W}$ denotes the specific form of U close to the black and white horizon, respectively, and $\mathcal{U}_{B,W}$ are analytic functions. Putting Eq. (10) into the above expression,

$$U_{B,W} = p(u \to \pm\infty) = \mathcal{P}_{B,W}(e^{\mp\kappa u}), \tag{13}$$

where $\mathcal{P}_{B,W}$ are analytic functions. Close to the horizons $u \to \pm\infty$, thus $e^{\mp\kappa u} \to 0$ and p can be expanded as

$$U = p(u \to \pm\infty) = U_{B,W} \mp A_{B,W} e^{\mp\kappa u} + O\left(e^{\mp 2\kappa u}\right), \tag{14}$$

where $A_{B,W}$ are positive constants. This asymptotic behavior of rightgoing rays is apparent from Fig. 4 (solid lines). It yields exponential separation of null geodesic close to the black horizon and exponential accumulation close to the white horizon.

It is worth stressing that this result is completely general. The asymptotic form of $U = p(u)$ does not depend on the details of $\hat{v}$, but only on its early- and late-time behaviors, corresponding to a Minkowskian spacetime at and to a stationary warp-drive spacetime, respectively.

Analogously, one can find the relation between the early- and late-times null coordinates W and w, associated with leftgoing light rays, which are solutions of

$$\frac{\mathrm{d}r}{\mathrm{d}t} = -c + \hat{v}(r, t). \tag{15}$$

In this case, leftgoing rays can cross the horizons, propagating from $\mathscr{I}_R^-$ to $\mathscr{I}_L^+$ (see Figs. 3 and 4). As a consequence, both W and w are defined in the asymptotic regions L and R outside the bubble. For instance,

$$W(t \to -\infty) = t + \frac{r}{c}. \tag{16}$$

However, in place of w, it is more convenient to use a different coordinate $\tilde{w}$, defined inside the bubble in analogy with Eq. (7),

$$d\tilde{w} = dt + \frac{dr}{c - \bar{v}(r)}. \tag{17}$$

It is easy to show [11] that the relation $W = q(\tilde{w})$ is always regular, as illustrated in Fig. 4 by the non-singular behavior of leftgoing null geodesics (dashed lines).

3 Particle production and renormalized stress-energy tensor

In a black hole geometry an exponential relation $p(U)$ between u and U, as in Eq. (14), allows to conclude that Hawking radiation is emitted with temperature $\kappa/2\pi$. However, in the case of warp drives, its implications for particle production are not straightforward because late-time modes labeled by u are not standard plane waves [see Eq. (10)]. Only if κ is large enough that the typical wavelength of the emitted radiation is much smaller than the bubble size, then a plane-wave approximation is allowed in the center of the bubble. In this case, it is possible to conclude that standard Hawking radiation at temperature T is emitted at late times. To obtain more significant information, also close to the horizons, we therefore consider the behavior of the RSET.

To calculate the RSET inside the warp-drive bubble we follow the method proposed in [17]. The metric can be written as

$$ds^2 = -C(U, W)dU dW. \tag{18}$$

or, using the null coordinates u and $\tilde{w}$, as

$$ds^2 = -\bar{C}(u, \tilde{w})du d\tilde{w} , \quad C(U, W) = \frac{\bar{C}(u, \tilde{w})}{\dot{p}(u)\dot{q}(\tilde{w})}, \tag{19}$$

where $U = p(u)$ and $W = q(\tilde{w})$. Following Ref. [11], we refer to the RSET associated with a single quantum massless scalar field. Its components are [16]:

$$T_{UU} = -\frac{1}{12\pi}C^{1/2}\partial_U^2 C^{-1/2}, \tag{20}$$

$$T_{WW} = -\frac{1}{12\pi}C^{1/2}\partial_W^2 C^{-1/2}, \tag{21}$$

$$T_{UW} = T_{WU} = \frac{1}{96\pi}C R. \tag{22}$$

In the presence of other fields, the previous expressions have to be corrected only by a multiplicative numerical factor. The RSET components in the stationary region inside the bubble are directly computed by using the relationships $U = p(u)$ and $W = q(\tilde{w})$, introduced in Sec. 2.2.

Significant physical information is extracted from the RSET by studying, for instance, the energy density ρ measured by a set of freely falling observers, with four velocity $u^\mu = (1, \bar{v})$ in (t, r) coordinates,

$$\rho = T_{\mu\nu}u_c^\mu u_c^\nu, \tag{23}$$

which is conveniently expressed as the sum of three terms,

$$\rho = \rho_{\text{st}} + \rho_{\text{dyn}-u} + \rho_{\text{dyn}-\tilde{w}}. \tag{24}$$

The first static term

$$\rho_{\text{st}} \equiv -\frac{1}{24\pi} \left[\frac{\left(\bar{v}^4 - \bar{v}^2 + 2\right)}{\left(1 - \bar{v}^2\right)^2} \bar{v}'^2 + \frac{2\bar{v}}{1 - \bar{v}^2} \bar{v}'' \right] \tag{25}$$

depends only on the r coordinate through $\bar{v}(r)$ and represent vacuum polarization. The two dynamical terms

$$\rho_{\text{dyn}-u} \equiv \frac{1}{48\pi} \frac{f(u)}{(1 + \bar{v})^2}, \tag{26}$$

$$\rho_{\text{dyn}-\tilde{w}} \equiv \frac{1}{48\pi} \frac{g(w)}{(1 - \bar{v})^2} \tag{27}$$

depend also on u ($\tilde{w}$) and correspond to the energy carried by rightgoing (leftgoing) rays, which is red/blue-shifted by a term depending on r. To keep the notation compact we have put $c = 1$ and we have defined

$$f(u) \equiv \frac{3\ddot{p}^2(u) - 2\dot{p}(u)\,\dddot{p}(u)}{\dot{p}^2(u)}, \tag{28}$$

$$g(\tilde{w}) \equiv \frac{3\ddot{q}^2(\tilde{w}) - 2\dot{q}(\tilde{w})\,\dddot{q}(\tilde{w})}{\dot{q}^2(\tilde{w})}. \tag{29}$$

In Fig. 5, we present the result of the calculation of ρ inside the bubble [12], for a warp-drive geometry defined by the velocity profile introduced in Eq. (3). With this choice, the surface gravity is $\kappa = \sqrt{3}/2$ and the horizons appear at $t_H = 1$. The energy density ρ (thick solid line) of Eq. (23) is plotted as a function of r at different times ($t = 0.5, 1, 2, 3$) and r varies between r_B and r_W, the locations of $\mathcal{H}_W$ and $\mathcal{H}_B$. The three terms ρ_{st}, $\rho_{\text{dyn}-u}$, and $\rho_{\text{dyn}-w}$, defined in Eqs. (25), (26), and (27), are plotted with thin-solid, dashed, and dot-dashed lines, respectively.
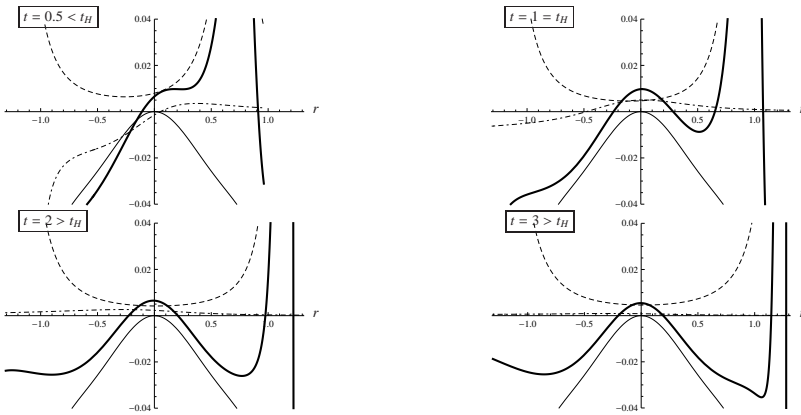

Figure 5. Energy density ρ (thick solid line), ρ_{st} (solid line), $\rho_{\text{dyn}-u}$ (dashed line) and $\rho_{\text{dyn}-w}$ (dot-dashed line) as functions of r, $r_B < r < r_W$ at time $t = 0.5, 1, 2, 3$. The horizons form at $t_H = 1$.

This figure shows that the dynamic term $\rho_{\mathrm{dyn}-w}$ (dot-dashed line) is transient and gives an important contribution only during the process of formation of the warp-drive bubble. In fact, $g(\tilde{w})$ differs from 0 only for values of $\tilde{w}$ corresponding to light rays crossing the bubble at $t \sim t_H$. At late time instead $\dot{q}(\tilde{w})$ goes to a constant and $g(\tilde{w}) \to 0$. Thus, $\rho_{\mathrm{dyn}-w}$ can be safely neglected at late times.

RSET in the center of the bubble.

In the center of the bubble ($r = 0$) $\rho_{\mathrm{st}} = 0$, because $\bar{v}(r = 0) = \bar{v}'(r = 0) = 0$. At late times when $\rho_{\mathrm{dyn}-w}$ is negligible, the only contribution to the energy density is given here by $\rho_{\mathrm{dyn}-u}$. Moreover, since $u(t, 0) \to +\infty$, $\rho_{\mathrm{dyn}-u}$ can be evaluated by expanding $f(u)$ at large values of u, $f(u \to \infty) = \kappa^2$. Finally $\rho(r = 0) \approx \kappa^2/(48\pi)$. This is the energy density $\pi T_{\mathrm{H}}^2/12$ of a scalar field in $1 + 1$ dimensions at the Hawking temperature $T_{\mathrm{H}} = \kappa/2\pi$. Using $\kappa = \sqrt{3}/2$, the energy density is $\rho \approx \kappa^2/48\pi \approx 0.005$, which coincides with the numerical results at late times ($t = 3$), shown in the bottom panel of Fig. 5.

Note that the Hawking temperature of this radiation is huge, $T_{\mathrm{H}} \sim \kappa \gtrsim 10^{-2}\, T_{\mathrm{P}}$, where T_{P} is the Planck temperature, about 10^{32} K, when QI are assumed [6, 8]. Indeed, the wall thickness for a warp drive with $v_0 \approx c$ would be $\Delta \lesssim 10^2\, L_{\mathrm{P}}$, and its surface gravity $\kappa \gtrsim 10^{-2}\, t_{\mathrm{P}}^{-1}$, where t_{P} is the Planck time. If instead the warp drive is supported by matter violating QI, such a high temperature can be avoided. For instance, with $\Delta \sim 1$ m, the temperature is about 0.003 K (corresponding to a wavelength of 1 m).

RSET on the black, white, and Cauchy horizons.

On the horizons $r = r_{B,W}$, both ρ_{st} and $\rho_{\mathrm{dyn}-u}$ diverge. Indeed the term $(1 + \bar{v})$ in the denominators of Eqs. (25) and (26) vanishes at $r = r_{B,W}$. By expanding $f(u)$ for $u \to \pm\infty$ in ρ_{st} and $\rho_{\mathrm{dyn}-u}$, one finds that the diverging terms exactly cancel each other [11] and the total ρ does not diverge, in agreement with the Fulling-Sweeny-Wald theorem [18]. Furthermore, the subleading terms yield

$$\rho\left(r \simeq r_{B,W}\right) = C_{B,W} + B_{B,W}e^{\mp 2\kappa t} + O\left(r - r_{B,W}\right). \tag{30}$$

This contribution is exponentially damped on the black horizon, on a time scale $\sim 1/\kappa$, as shown in Fig. 5. The same behavior characterizes the RSET on the horizon of a black hole formed through the gravitational collapse of a star [17]. Conversely, on the white horizon the subleading term exponentially grows with time. That is, moving along $\mathscr{H}_W$, ρ grows exponentially and diverges at the crossing point between $\mathscr{H}_W$ and $\mathscr{H}_C^+$, as shown in Fig. 5, where the value of ρ (thick solid line) at $r = r_W$ goes towards $-\infty$ as $t \to +\infty$.

Finally, a positive energy pulse, whose value at the peak diverges with time to $+\infty$, approaches r_W as $r - r_W \propto e^{-\kappa t}$. Thus, ρ diverges in two different ways for $r \to r_W$ and $t \to \infty$, depending on the order in which the two limits are taken. To understand the physical meaning of these divergences it is convenient to consider the Penrose diagram of Fig. 3, where the location ($r = r_W, t = +\infty$) is represented by a whole line ($\mathscr{H}_C^+$ and $\mathscr{H}_R^+$) rather than by a single point. The former negative divergence appears by first taking the limit $r \to r_W$ and afterwards moving on the white horizon $\mathscr{H}_W$ toward the crossing point between $\mathscr{H}_W$ and $\mathscr{H}_C^+$ (late-time limit). The latter positive divergence appears instead by fixing a value of u and moving on the corresponding geodesic, which is parallel to $\mathscr{H}_B$ and $\mathscr{H}_W$ in the Penrose diagram, until the Cauchy horizon $\mathscr{H}_C^+$ is reached. Note that these results do not contradict the Fulling-Sweeny-Wald theorem [18], since both divergences take place on a Cauchy horizon.

Furthermore, the natures of these two divergences are quite different. The divergence at the crossing point between $\mathscr{H}_W$ and $\mathscr{H}_C^+$ is intrinsically due to the inevitable transient disturbances produced by the formation of the white horizon. On the contrary, the divergence on $\mathscr{H}_C^+$ is due to the infinite

blue-shift suffered by light rays as they approach the Cauchy horizon and it is similar to the often claimed instability of inner horizons in Kerr-Newman black holes [19–21].

However, in both cases these effects produce an exponential growth of the RSET, whose backreaction dooms the warp drive to be semiclassically unstable on a time scale of the order of $1/\kappa$, the inverse of the surface gravity of the white horizon. By QI inequalities, this timescale would be of the order of 10^2 Planck times, about 10^{-42} s. Even violating the QI, to get a time scale of 1 s, a wall as large as 3×10^8 m is needed. Thus, most probably, one would be able to maintain a warp drive with superluminal speed for a very short interval of time.

4 Warp drives in Lorentz violating theories

In the previous section we showed that superluminal warp-drive geometries are quantum mechanically unstable. However, that analysis rested on relativistic quantum field theory. Thus, one should examine whether the warp-drive instability is peculiar to the assumed local Lorentz symmetry. Indeed, it is known that non-linear dispersion relations remove Cauchy horizons and regulate the fluxes emitted by white holes [14]. Moreover, although observations constrain to ultra high energy a possible breaking of that symmetry [22], one cannot definitely exclude ultraviolet violations of the local Lorentz symmetry, which have been suggested by several investigations [23–25].

A stability analysis of warp-drive configurations with Lorentz violation was performed in [13] in a 1+1 dimensional stationary system, by considering a massless scalar field with quartic dispersion relation propagating on a geometry defined by the line element of Eq. (2). If the Lorentz symmetry is violated, it is sufficient to consider stationary warp drives, because in this case the Cauchy horizons are not present and the initial quantum state can be properly defined without ambiguities. In this spacetime ∂_t is therefore a globally defined Killing vector field, which is time-like within the bubble (region C) and space-like outside (regions L and R, see Fig. 1). The action of this scalar fields is

$$S_\pm = \frac{1}{2} \int d^2 x \sqrt{-g} \left[g^{\mu\nu} \partial_\mu \phi \partial_\nu \phi \pm \frac{(h^{\mu\nu} \partial_\mu \partial_\nu \phi)^2}{\Lambda^2} \right], \tag{31}$$

where $h^{\mu\nu} = g^{\mu\nu} + u^\mu u^\nu$ is the spatial metric on a section orthogonal to some unit time-like vector field u^μ, which specifies the preferred frame used to implement the dispersion relation [26]. In the present settings u^μ should be given from the outset, while in condensed matter the preferred frame is fixed by the fluid flow [27]. Inspired by this analogy, we choose u^μ to be $(1, \bar{v})$ in the (t, r) frame. This u^μ flow is geodesic and asymptotically at rest in the (t, x) frame of Eq. (1), so that stationarity is preserved. The sign $\pm$ in Eq. (31) holds for superluminal dispersion (velocity of high momentum photons larger than velocity c of low momentum photons) and subluminal dispersion (velocity of high momentum photons smaller than c), respectively. With the metric of Eq. (2), the wave equation generated by the above action is

$$\left[(\partial_t + \partial_r \bar{v}) (\partial_t + \bar{v} \partial_r) - \partial_r^2 \pm \frac{1}{\Lambda^2} \partial_r^4 \right] \phi = 0. \tag{32}$$

Because of stationarity, the field can be decomposed in eigenfrequency modes $\phi = \int d\omega \, e^{-i\omega t} \phi_\omega$, where ω is the conserved frequency (with respect to the Killing time). Correspondingly, at fixed ω the dispersion relation reads

$$(\omega - \bar{v} k_\omega)^2 = k_\omega^2 \pm \frac{k_\omega^4}{\Lambda^2} \equiv \Omega_\pm^2, \tag{33}$$

where k_ω is the spatial wave vector, and Ω is the *comoving* frequency, measured in the proper frame defined by the flow u^μ. Equation (33) is graphically solved in Fig. 6.
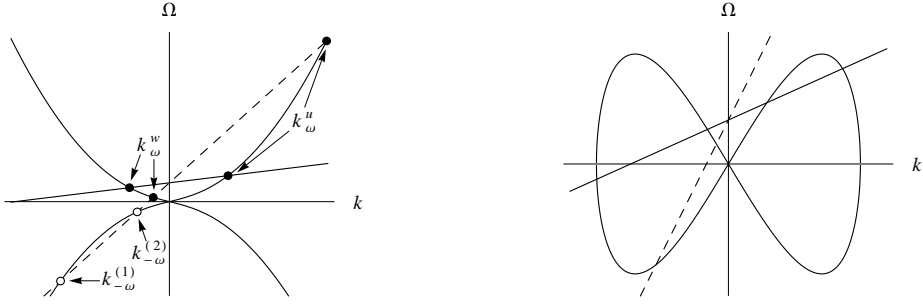
Figure 6. Graphical solution of Eq. (33) for super (top panel), and subluminal dispersion (bottom panel). In both panels, the straight lines represent $\omega - \bar{v}k$ for $|\bar{v}| < 1$ (solid) and $|\bar{v}| > 1$ (dashed). The curved lines represents $\pm\Omega_\pm(k)$. On the left, closed (open) dots refer to roots with positive (negative) Ω_+ which correspond to positive (negative) norm modes.

For superluminal dispersion (top panel) and $|\bar{v}| < 1$ (solid line), that is in region C, there are two real roots k_ω^w and k_ω^u (closed dots), describing leftgoing and rightgoing waves φ_ω^w and φ_ω^u, respectively, and two complex roots $k_\omega^\uparrow$ and $k_\omega^\downarrow$, describing a spatially growing and decaying mode, $\varphi_\omega^\uparrow$ and $\varphi_\omega^\downarrow$, respectively. The superscripts u and w have been chosen accordingly to the notation introduced in Sec. 2.2. Indeed, in the relativistic limit $\Lambda \to \infty$, the modes φ_ω^u and φ_ω^w propagate on the geodesics of Fig. 4. For $|\bar{v}| > 1$ (dashed line), that is in regions L and R, for values of ω smaller than a cut-off frequency $\omega_{\max}$ [14], the two complex roots turn into real ones, $k_\omega^{(1)}$ and $k_\omega^{(2)}$ (open dots), with negative Ω. Correspondingly there exist two additional propagating waves $\varphi_{-\omega}^{(1)}$ and $\varphi_{-\omega}^{(2)}$ with negative norm.

If the dispersion relation is subluminal (bottom panel), there are instead four real-k solutions in region C, where $|\bar{v}| < 1$, and two real-k and two complex-k solutions in regions L and R, where $|\bar{v}| > 1$. Consequently, there are now two extra propagating modes which are trapped inside the warp-drive bubble.

4.1 Superluminal dispersion relation

In this case, in each of the two infinite asymptotic external regions L and R, there are 4 propagating modes for each $\omega < \omega_{\max}$. Therefore 8 asymptotically bounded modes [14] can be defined. By examining their asymptotic behaviors those modes are grouped in two bases, named *in* and *out*. Each incoming mode $\phi_\omega^{(i),\text{in}}$, belonging to the *in* basis (outgoing mode $\phi_\omega^{(i),\text{out}}$, belonging to the *out* basis) possesses a single asymptotic branch $\varphi_\omega^{(i),L/R}$ carrying unit current and with group velocity directed towards region C (from C to ∞). The construction of the incoming mode $\phi_{-\omega}^{(1),\text{in}}$ is exemplified in Fig. 7.

When the dispersive scale and the horizon surface gravity κ are well separated ($\omega \sim \kappa \ll \Lambda$), the leftgoing mode w does not significantly mix with the other three modes, all defined on the rightgoing branch of Eq. (33) [28], as numerically checked in Ref. [14]. Thus, the scattering matrix relating the *in* and *out* bases is effectively 3×3,

$$
\begin{pmatrix} \phi_\omega^{u,\text{in}} \\ \left(\phi_{-\omega}^{(1),\text{in}}\right)^* \\ \left(\phi_{-\omega}^{(2),\text{in}}\right)^* \end{pmatrix} = \begin{pmatrix} \alpha_\omega^u & \beta_{-\omega}^{(1)} & \beta_{-\omega}^{(2)} \\ \beta_\omega^{(1)} & \alpha_{-\omega}^{(1)} & A_{-\omega} \\ \beta_\omega^{(2)} & \tilde{A}_{-\omega} & \alpha_{-\omega}^{(2)} \end{pmatrix} \begin{pmatrix} \phi_\omega^{u,\text{out}} \\ \left(\phi_{-\omega}^{(1),\text{out}}\right)^* \\ \left(\phi_{-\omega}^{(2),\text{out}}\right)^* \end{pmatrix}. \tag{34}
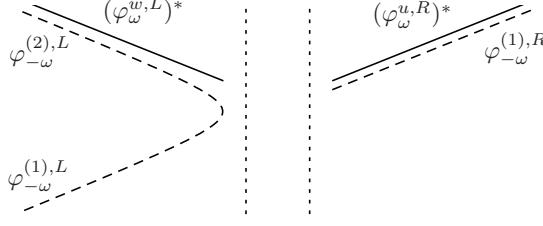$$

Figure 7. Asymptotic decomposition in plane waves $\varphi_\omega^{(i),L/R}$ of the incoming mode $\phi_{-\omega}^{(1),\text{in}}$. Note that only $\varphi_{-\omega}^{(1),L}$ has group velocity directed toward the horizons, with wavevector $k_\omega^{(1)}$.

Since the norms of $\phi_{-\omega}^{(i),\text{in/out}}$ are negative, the coefficients of this scattering matrix satisfy anomalous normalizations conditions, such as

$$|\alpha_\omega^u|^2 - |\beta_\omega^{(1)}|^2 - |\beta_\omega^{(2)}|^2 = 1. \tag{35}$$

The information about spontaneous particle production is all encoded in the scattering matrix. For instance, if the system is in a quantum state which is vacuum at early times, that is the occupation numbers of incoming modes vanish, then the mean occupation numbers of outgoing particles is fixed by the coefficients of this matrix:

$$\bar{n}_{-\omega}^{(i)} = |\beta_{-\omega}^{(i)}|^2, \tag{36}$$

$$\bar{n}_\omega^u = \bar{n}_{-\omega}^{(1)} + \bar{n}_{-\omega}^{(2)}, \tag{37}$$

where $n_{-\omega}^{(i)}$ are the occupation numbers of the outgoing negative frequency modes $\phi_{-\omega}^{(i),\text{out}}$ and n_ω^u is the occupation number of the positive frequency mode $\phi_\omega^{u,\text{out}}$, which is related to $n_{-\omega}^{(i)}$ by energy conservation.

The coefficients of Eq. (34) can be computed using connection formula techniques [28] when the surface gravity κ is much smaller than the dispersive scale Λ. We first expand the field ϕ_ω in both asymptotic regions L and R as a sum of plane waves:

$$\begin{aligned}
\phi_\omega &= L_\omega^u \varphi_\omega^{u,L} + L_\omega^{(1)}(\varphi_{-\omega}^{(1),L})^* + L_\omega^{(2)}(\varphi_{-\omega}^{(2),L})^*, \\
\phi_\omega &= R_\omega^u \varphi_\omega^{u,R} + R_\omega^{(1)}(\varphi_{-\omega}^{(1),R})^* + R_\omega^{(2)}(\varphi_{-\omega}^{(2),R})^*,
\end{aligned} \tag{38}$$

where we have neglected the leftgoing modes $\varphi_\omega^{w,L/R}$. The coefficients appearing in this expansions are connected by

$$\begin{pmatrix} R_\omega^u \\ R_\omega^{(1)} \\ R_\omega^{(2)} \end{pmatrix} = U_W \cdot U_{\text{WKB}} \cdot U_B^{-1} \cdot \begin{pmatrix} L_\omega^u \\ L_\omega^{(1)} \\ L_\omega^{(2)} \end{pmatrix}, \tag{39}$$

where U_B and U_W respectively describe the scattering on the black and white horizons [28] and U_{WKB} describes the WKB propagation from one horizon to the other. It contains the exponential of $iS_\omega^a = i \int dx\, k_\omega^a(x)$, where k_ω^a is k_ω^u, $k_\omega^\uparrow$ or $k_\omega^\downarrow$. Note that, since $k^\uparrow$ has negative imaginary part, $e^{iS_\omega^\uparrow}$ is exponentially large, growing as $e^{\Lambda(r_W - r_B)}$. Analogously $e^{iS_\omega^\downarrow}$ is exponentially small because $k^\downarrow = k^{\uparrow *}$.

This formalism allows to determine the coefficients of the expansion of the incoming modes on the *out* basis. As an example, we illustrate how to compute the coefficients of the expansion of $\phi_{-\omega}^{(1),\text{in}}$, which form the second row of the scattering matrix of Eq. (34). As shown in Fig. 7, $\phi_{-\omega}^{(1),\text{in}}$ is

constructed by imposing that the amplitude $L_\omega^{(1)}$ of the branch $\varphi_{-\omega}^{(1),L}$ equals 1 and that the amplitudes L_ω^u and $R_\omega^{(2)}$ of the branches $\varphi_\omega^{u,L}$ and $\varphi_{-\omega}^{(2),R}$ vanish [see Eq. (38)]. Moreover, the coefficients associated with the outgoing modes are $R_\omega^u = \beta_\omega^{(1)}$, $R_\omega^{(1)} = \alpha_{-\omega}^{(1)}$, and $L_\omega^{(2)} = A_{-\omega}$. The connection formula (39) yields

$$\begin{pmatrix} \beta_\omega^{(1)} \\ \alpha_{-\omega}^{(1)} \\ 0 \end{pmatrix} = U_W \cdot U_{\text{WKB}} \cdot U_B^{-1} \cdot \begin{pmatrix} 0 \\ 1 \\ A_{-\omega} \end{pmatrix}. \tag{40}$$

This is a system of three equations with three unknowns, whose solution is

$$\begin{aligned} \beta_\omega^{(1)} &= \tilde{\beta}_\omega^B \times e^{iS_\omega^u} \times \alpha_\omega^W + O(e^{iS_\omega^\downarrow}), \\ \alpha_{-\omega}^{(1)} &= -\tilde{\beta}_\omega^B \times e^{iS_\omega^u} \times \beta_\omega^W + O(e^{iS_\omega^\downarrow}), \\ A_{-\omega} &= \tilde{\alpha}_\omega^B, \end{aligned} \tag{41}$$

where the α's and β's in the right-hand sides of the above expressions are the standard Bogoliubov coefficients for black and white holes [29]. All the other coefficients of Eq. (34) are computed by applying a similar analysis to the other two incoming modes. Surprisingly, the exponentially large factor $e^{\Lambda(r_W - r_B)}$ cancels out from all the coefficients, although the non-positive-definite conservation law of Eq. (35) does not bound them. The leading terms of these coefficients are therefore given by the coefficients of U_B and U_W [28], times some phase generated by the propagation in region C. Thus, $\beta_\omega^{(1)}$ and $\alpha_{-\omega}^{(1)}$ are given by the product of a coefficient of U_B, a coefficient of U_W, and a propagation phase. Indeed the semi-classical trajectories associated with the conversion of the incoming mode $\phi_{-\omega}^{(1),\text{in}}$ into the outgoing modes $\phi_\omega^{u,\text{out}}$ and $\phi_{-\omega}^{(1),\text{out}}$, respectively, pass through both horizons. Instead, $A_{-\omega}$ is given by only one coefficient of U_B, because the semi-classical trajectory associated with the conversion of $\phi_{-\omega}^{(2),\text{in}}$ into the outgoing mode $\phi_{-\omega}^{(2),\text{out}}$ involves only a reflection on the black horizon.

The physical consequences of the behavior of the coefficients of the scattering matrix can be analyzed by computing the expectation value of the stress-energy tensor

$$T_{\mu\nu} \equiv \frac{2}{\sqrt{-g}} \frac{\delta S_+}{\delta g^{\mu\nu}} = T_{\mu\nu}^{(0)} + T_{\mu\nu}^{(\Lambda)}, \tag{42}$$

where $T_{\mu\nu}^{(0)}$ is the standard relativistic expression and $T_{\mu\nu}^{(\Lambda)}$ arises from the Lorentz violating term of the action,

$$T_{\mu\nu}^{(\Lambda)} = \frac{1}{\Lambda^2} \left[h^{\alpha\beta} \left(\phi_{,\alpha\beta}\phi_{,\mu\nu} + \phi_{,\mu\nu}\phi_{,\alpha\beta} \right) - \frac{1}{2} \left(h^{\alpha\beta}\phi_{,\alpha\beta} \right)^2 g_{\mu\nu} \right]. \tag{43}$$

As usual, the above expression has to be renormalized. To this aim, we expand the field in the asymptotic region on the right of the white horizon as the superposition of the two rightgoing modes $\phi_\omega^{u,\text{out}}$ and $\phi_{-\omega}^{(1),\text{out}}$ (see Fig. 7),

$$\phi = \int d\omega \left[\phi_\omega^{u,\text{out}}\hat{a}_\omega^{u,\text{out}} + \phi_{-\omega}^{(1),\text{out}}\hat{a}_{-\omega}^{(1),\text{out}} \right] + \text{h.c.} \tag{44}$$

In this region, the geometry is stationary and homogeneous. Hence the renormalized tensor $T_{\mu\nu}^{\text{ren}}$ is obtained by standard normal ordering of the above creation and destruction operators of outgoing modes. Choosing a quantum state which is vacuum at early times, $\langle 0_{\text{in}} | T_{\mu\nu}^{\text{ren}} | 0_{\text{in}} \rangle$ is computed by using Eq. (34). The final expression is an integral over ω of a sum of terms, each being the product of two modes $\phi_\omega^{u,\text{out}}$ and $\phi_{-\omega}^{(1),\text{out}}$ and of two coefficients of the scattering matrix.

We consider now only the asymptotic behavior of these terms in Fourier space, since this is enough to identify possible divergences. First note that there are no ultraviolet divergent terms, because the β

coefficients of Eq. (34) vanish and no negative frequency modes are present for $\omega > \omega_{\max}$. Therefore divergences can possibly appear only in the infrared domain.

In each term of $T_{\mu\nu}^{(0)}$ there are two derivatives with respect to t or r, producing two powers of ω, $k_\omega^{(u)}$ or $k_\omega^{(1)}$ in Fourier space. Analogously, in $T_{\mu\nu}^{(\Lambda)}$ four powers of frequency and momentum appear. In region R (see Fig. 6), in the limit $\omega \to 0$, the wavenumbers $k_\omega^{(u)}, k_\omega^{(1)}$ go to constant opposite values that we call k_0 and $-k_0$, respectively. For this reason, terms containing only spatial derivatives are not suppressed when $\omega \to 0$. The leading terms in the non-dispersive component of the RSET, $\langle 0_{\mathrm{in}}|T_{\mu\nu}^{(0),\,\mathrm{ren}}|0_{\mathrm{in}}\rangle$, are therefore proportional to

$$\frac{k_0^2}{4\pi\Omega(k_0)\,v_{g0}} \int \mathrm{d}\omega \left[\bar{n}_\omega^{(u)} + \bar{n}_{-\omega}^{(1)}\right]. \tag{45}$$

This expression gives the integrated occupation number of the two outgoing species and v_{g0} is their asymptotic group velocity in the (t, r) frame. The leading terms in the dispersive component of the RSET, $\langle 0_{\mathrm{in}}|T_{\mu\nu}^{(\Lambda),\,\mathrm{ren}}|0_{\mathrm{in}}\rangle$, are proportional to Eq. (45) up to an extra factor of k_0^2/Λ^2. Since $k_0 = \Lambda\sqrt{v_0^2 - 1}$, the contribution of the (0) and (Λ) components of the RSET are typically of the same order.

Finally, the key result comes from the fact that $|\beta_\omega^{(1)}|^2$ diverges as $1/\omega^2$ for $\omega \to 0$, being the product of the two coefficients $|\beta_\omega^B|^2 \sim 1/\omega$ and $|\beta_\omega^W|^2 \sim 1/\omega$ of the scattering matrix of the black hole and of the white hole, respectively (this infrared behavior has been validated by numerical analysis). Then, if the warp drive is created at some time t_H, only frequencies $\omega > 1/T$, with $T \equiv t - t_H$, contribute to the emitted spectrum at time t. This provides an infrared cutoff to the integral of Eq. (45). Thus, the emitted energy density scales as

$$\mathcal{E} \propto \Lambda \int_{1/T} \mathrm{d}\omega \left[\bar{n}_\omega^{(u)} + \bar{n}_{-\omega}^{(1)}\right] \propto \Lambda\kappa^2 T. \tag{46}$$

That is, the infrared divergence of the spectrum leads to a linear growth of $\mathcal{E}$. We now compare this result with that of Ref. [30]. In that work, the spontaneous emission of phonons from an analog white hole is investigated in a Bose–Einstein condensate, where the dispersion relation of phonons is identical to the superluminal one of Eq. (33). In that system the spontaneously emitted flux diverges logarithmically with time when the initial quantum state is vacuum, linearly when the initial state is thermal. In a warp-drive geometry, even if the initial state is vacuum, the black hole horizon emits thermal radiation. The white hole horizon is then stimulated by this emission as if a thermal distribution were initially present and the emitted flux eventually grows linearly, in agreement with Ref. [30].

Using quantum inequalities [7], the typical time scale of this linear growth is of the order of the Planck time t_P (unless Λ is very different from t_P^{-1}) since $\kappa \lesssim 10^{-2} t_P^{-1}$. Our analysis leads to the conclusion that even in the presence of superluminal dispersion, warp drives are still unstable on a short time scale.

4.2 Subluminal dispersion relation

If the dispersion relation is subluminal (minus sign in front of the quartic term in Eq. (33), bottom panel of Fig. 6) there are two extra propagating norm modes which are trapped in region C. Hence they bounce back and forth, inducing an exponential amplification of the emitted radiation. This phenomenon is the subluminal version of the black hole laser effect [31]. As a result, the asymptotic fluxes and therefore $\langle 0_{\mathrm{in}}|T_{\mu\nu}^{\mathrm{ren}}|0_{\mathrm{in}}\rangle$ grow exponentially with time.

This dynamical instability is described by a discrete set of complex-frequency eigenmodes that are asymptotically bounded [32, 33]. In the original version, the analysis was performed with a superluminal dispersion relation in a spacetime with a velocity profile similar to the warp-drive one (Fig. 1), but where the external and internal regions are exchanged ($|v| < 1$ in regions L and R; $|v| > 1$ in region C). However, there is a precise symmetry between the two cases [28], consisting in changing both the sign of the dispersion relation and that of $\bar{v} + c$. This symmetry allows to infer that the set of complex eigenfrequencies governing the laser instability share the same features in both configurations.

Thus, also when the Lorentz violation is implemented through a subluminal dispersion relation, superluminal warp drives are still unstable.

5 Conclusions

This contribution summarizes the semiclassical stability analysis of warp-drive spacetimes in both Lorentz-invariant and Lorentz-violating quantum field theories, performed in Refs. [11–13]. In these works a 1 + 1 calculation was performed. Generally in spherically symmetric spacetimes this could be seen as an s-wave approximation to the exact results. However, this is not the case for the axisymmetric warp-drive configuration. Nonetheless, we do expect that the salient features of those results would be maintained in a full 3+1 calculation, given that they will still be valid in a suitable open set of the horizons centered around the axis aligned with the direction of motion.

First, we investigated the causal properties of the superluminal warp-drive geometry in the context of standard general relativity, constructing its Penrose diagram. As seen by an observer inside the warp-drive bubble, the front and the rear wall of the bubble behave as a white and a black hole horizon, respectively. In eternal warp drives a past and a future Cauchy horizons are also present. Because of the presence of the past Cauchy horizon, the choice of a proper initial state is ambiguous. To solve this problem, we considered a more realistic configuration of a warp drive dynamically created out of an initially Minkowski space time. In this case the past horizon is removed and the initial quantum state is well-defined. Then, we studied the properties of spontaneous particle production for a scalar field living on this geometry by computing its renormalized stress energy tensor. We briefly summarize the results of this analysis.

(1) Hawking-like radiation is generated at the rear wall of the warp-drive bubble, corresponding to a black hole horizon. By QI [6, 8], the wall thickness is extremely small and the surface gravity is huge. Hence, the Hawking temperature of this radiation is huge, $T_{\rm H} \sim \kappa \gtrsim 10^{-2} T_{\rm P}$, where $T_{\rm P}$ is the Planck temperature, about 10^{32} K.

(2) The formation of a white horizon produces a radiation which accumulates on the white horizon itself. This causes the energy density ρ measured by a freely falling observer to grow unboundedly with time on this horizon.

(3) The formation of a future Cauchy horizon gives rise to an instability, similar to the instability of inner horizons in black holes, due to the blueshift of Hawking radiation produced by the black horizon.

The time scale of both instabilities is of the order of the inverse of the surface gravity, about 10^2 Planck times, if QI are assumed. However, even without this assumption, this time scale remains very short. Indeed, to get a time scale of 1 s, the wall should be as thick as 3×10^8 m. The semiclassical backreaction of the RSET will make the superluminal warp drive rapidly unstable. Thus, superluminal speed can be maintained for a very short time.

Finally, we re-examined the stability properties of warp drives taking into account possible violations of the Lorentz symmetry at high momenta. Even if in this case the Cauchy horizon is removed,

superluminal warp drives are still unstable, but the type of instability is very different, depending on the form of the dispersion relation.

(1) If the dispersion relation is superluminal (velocity of high momentum photons larger than velocity c of low momentum photons), the renormalized stress-energy tensor grows linearly with time on a short time scale.

(2) If the dispersion relation is subluminal there exists a propagating mode trapped in the interior of the bubble. This mode bounces back and forth between the black and the white horizon, originating the subluminal version of the black hole laser instability, which produces an exponentially growing flux of emitted particles.

In conclusion, the analysis presented in this contribution convincingly rules out the stability of superluminal warp drives at semiclassical level. Of course, all the aforementioned problems disappear when the bubble remains subluminal. In that case no horizon forms, no Hawking radiation is created, and neither high temperatures nor instabilities are found.

A suggestive interpretation of these results can be argued in connection with the so called chronology protection conjecture [34]. In fact, a time machine could be built through a couple of superluminal warp drives traveling in opposite directions [2]. Thus, a protection mechanism seems to act at an early stage, forbidding the creation of a system which could be dangerous for causality. Moreover, whereas former attempts to tackle the issue of chronology protection deeply relied on local Lorentz invariance [35], the present result suggests that this conjecture may be valid also for quantum field theories violating Lorentz invariance in the ultraviolet sector. It would be interesting to check whether all these results are general by applying a similar stability analysis to other spacetimes allowing superluminal travel, such as the Krasnikov tube [36, 37].

Acknowledgements

References

[1] M. Alcubierre, Class. Quant. Grav. **11**, L73 (1994)

[2] A.E. Everett, Phys. Rev. D **53**, 7365 (1996)

[3] F.S.N. Lobo (2007), arXiv:gr-qc/0710.4474

[4] F.S.N. Lobo, M. Visser, Class. Quant. Grav. **21**, 5871 (2004)

[5] F.S.N. Lobo, M. Visser (2004), arXiv:gr-qc/0412065

[6] M.J. Pfenning, L.H. Ford, Class. Quant. Grav. **14**, 1743 (1997)

[7] T.A. Roman, *Some Thoughts on Energy Conditions and Wormholes*, in *The Tenth Marcel Grossmann Meeting*, edited by M. Novello, S. Perez Bergliaffa, R. Ruffini (2005), p. 1909

[8] C. Van Den Broeck, Class. Quant. Grav. **16**, 3973 (1999)

[9] W.A. Hiscock, Class. Quant. Grav. **14**, L183 (1997)

[10] P.F. González-Díaz, Phys. Rev. D **62**, 044005 (2000)

[11] S. Finazzi, S. Liberati, C. Barcelo, Phys. Rev. D **79**, 124017 (2009)

[12] S. Finazzi, S. Liberati, C. Barceló, J. Phys.: Conf. Ser. **222**, 012046 (2010)

[13] A. Coutant, S. Finazzi, S. Liberati, R. Parentani, Phys. Rev. D **85**, 064020 (2012)

[14] J. Macher, R. Parentani, Phys. Rev. D **79**, 124008 (2009)

[15] C. Barceló, S. Liberati, S. Sonego, M. Visser, Class. Quant. Grav. **23**, 5341 (2006)

[16] N.D. Birrell, P.C.W. Davies, *Quantum Fields in Curved Space* (Cambridge University Press, 1984)

[17] C. Barcelo, S. Liberati, S. Sonego, M. Visser, Phys. Rev. D **77**, 044032 (2008)

[18] S.A. Fulling, M. Sweeny, R.M. Wald, Communications in Mathematical Physics **63**, 257 (1978)

[19] M. Simpson, R. Penrose, Int. J. Theor. Phys. **7**, 183 (1973)

[20] E. Poisson, W. Israel, Phys. Rev. D **41**, 1796 (1990)

[21] D. Marković, E. Poisson, Phys. Rev. Lett. **74**, 1280 (1995)

[22] S. Liberati, L. Maccione, Ann. Rev. Nucl. Part. Sci. **59**, 245 (2009)

[23] R. Gambini, J. Pullin, Phys. Rev. D **59**, 124021 (1999)

[24] T. Jacobson, D. Mattingly, Phys. Rev. D **64**, 024028 (2001)

[25] P. Hořava, Phys. Rev. D **79**, 084008 (2009)

[26] S. Corley, T. Jacobson, Phys. Rev. D **54**, 1568 (1996)

[27] W.G. Unruh, Phys. Rev. D **51**, 2827 (1995)

[28] A. Coutant, R. Parentani, S. Finazzi, Phys. Rev. D **85**, 024021 (2012)

[29] R. Brout, S. Massar, R. Parentani, P. Spindel, Phys. Rept. **260**, 329 (1995)

[30] C. Mayoral, A. Recati, A. Fabbri, R. Parentani, R. Balbinot, I. Carusotto, New J. Phys. **13**, 025007 (2011)

[31] S. Corley, T. Jacobson, Phys. Rev. D **59**, 124011 (1999)

[32] A. Coutant, R. Parentani, Phys. Rev. D **81**, 084042 (2010)

[33] S. Finazzi, R. Parentani, New J. Phys. **12**, 095015 (2010)

[34] S.W. Hawking, Phys. Rev. D **46**, 603 (1992)

[35] B.S. Kay, M.J. Radzikowski, R.M. Wald, Comm. Math. Phys **183**, 533 (1997)

[36] S.V. Krasnikov, Phys. Rev. D **57**, 4760 (1998)

[37] A.E. Everett, T.A. Roman, Phys. Rev. D **56**, 2100 (1997)